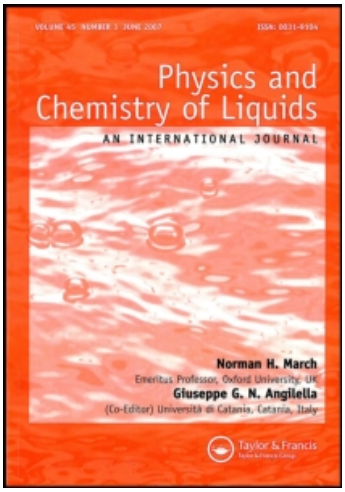

Physics and Chemistry of Liquids
Publication details, including instructions for authors and subscription information:
http://www.informaworld.com/smpp/title~content=t713646857

Transport Coefficients Of Ar—Kr Mixtures by Molecular Dynamics Computer Simulation

D. M. Heyes[a]; S. R. Preston[b]
[a] Department of Chemistry, University of Surrey, Guildford, UK [b] Department of Chemistry, Royal Holloway and Bedford New College, University of London, Egham, Surrey, UK

To cite this Article Heyes, D. M. and Preston, S. R.(1991) 'Transport Coefficients Of Ar—Kr Mixtures by Molecular Dynamics Computer Simulation', Physics and Chemistry of Liquids, 23: 3, 123 — 149
To link to this Article: DOI: 10.1080/00319109108027251
URL: http://dx.doi.org/10.1080/00319109108027251

Phys. Chem. Liq., 1991, Vol. 23, pp. 123–149
Reprints available directly from the publisher
Photocopying permitted by license only

TRANSPORT COEFFICIENTS OF Ar–Kr MIXTURES BY MOLECULAR DYNAMICS COMPUTER SIMULATION

D. M. HEYES

Department of Chemistry, University of Surrey, Guildford GU2 5XH, UK.

and

S. R. PRESTON

Department of Chemistry, Royal Holloway and Bedford New College, University of London, Egham, Surrey, TW20 0EX, UK.

(Received 12 November 1990)

Equilibrium molecular dynamics computer simulations have been used to determine the transport coefficients of model Ar–Kr mixtures, which are represented by Lennard-Jones pair potentials with Lorentz–Berthelot rules for the cross-species interactions. The component self-diffusion and mutual-diffusion coefficients are calculated from time correlation functions and mean square displacements. Time correlation functions are used to evaluate the shear and bulk viscosity, thermal conductivity and the thermal diffusion coefficient (Soret/Dufour coefficient). In the case of the thermal transport coefficients, the partial enthalpy of the two species is required at each state point to define the heat flux rigorously. We obtain this and the partial volume (and species resolved chemical potential) using particle-exchange (and particle insertion) techniques implemented in separate [NPT] simulations at the same state point.

The viscoelasticity of the fluids is characterised by the relaxation times for bulk and shear stress relaxation. The results are for dense liquids close to the triple point temperature and density. Agreement with experiment and previous simulation is particularly good for the density of the mixtures, the shear modulus, shear viscosity, shear stress relaxation time and thermal conductivity. As for the single component noble gas fluids (simulated and experiment) there is a significant qualitative difference in the temperature and, for mixtures, composition dependence of the bulk viscosity.

KEY WORDS: Binary mixtures, argon-krypton, MD, transport coefficients, Green–Kubo formulae.

1 INTRODUCTION

Transport coefficients in simple dense liquids can be calculated quantitatively by molecular dynamics using an appropriate time correlation function substituted into Green–Kubo integrand formulae[1–3]. There have been numerous MD studies of the transport coefficients of model simple liquids, following on from the pioneering work of Alder, Gass and Wainwright[4] for hard-sphere fluids, and Levesque, Verlet and Kurkijarvi[5] for Lennard-Jones fluids. A noteable recent computation is by Borgelt *et al.*[3], who used the Green–Kubo, GK, method to determine the self-diffusion coefficients, shear viscosity, bulk viscosity and thermal conductivity of a Lennard-Jones model for argon at numerous state points in the density range, 1.3–1.5 gcm^{-3}

and at temperatures between 100–300 K. Another recent publication, by Joslin *et al.*[6] reported equilibrium MD simulations of the bulk viscosity of attractive square well fluids (well-width equal to half the hard-core diameter) over a wide fluid range. In both of these studies comparisons with kinetic theory revealed only limited success. At present the only effective theoretical model for transport coefficients is by molecular dynamics simulation.

Non-equilibrium molecular dynamics, NEMD, is an alternative route to these transport coefficients. The transport coefficient is the ratio of a flux divided by the appropriate driving force. The linear transport coefficients (otherwise obtained by Green–Kubo in equilibrium MD) are determined by extrapolation of this apparent transport coefficient to zero driving force. (For shear viscosity, η_S, the flux is the shear stress and the driving force is the shear rate, $\dot{\gamma}$.) Again many applications of this method have been made[7–9] and its strengths and limitations are well-documented[10]. Broadly speaking, the two techniques involve comparable computational effort if only linear transport coefficients are required, and the choice of either is largely a matter of taste and inclination. Obviously, if non-newtonian phenomena are of interest then only the NEMD method is of use. An interesting, recent development is a reassessment of the triple point LJ viscosity to larger values than were currently accepted. This NEMD study has produced by $\gamma^{1/2}$ extrapolation, a value of 3.41 ± 0.07 in LJ reduced units rather than $\simeq 3.1 \pm 0.1$. This new value is closer to that obtained twenty years ago by Levesque *et al.*[5] using GK and largely in line with the value 3.6 ± 0.1 obtained by Heyes[11] using NEMD.

The simulation and experimental values for the self-diffusion coefficient, shear viscosity and thermal conductivity of the noble gas fluids are in agreement[12,13]. However, there still remains an unresolved discrepancy between the temperature and density dependence of the bulk viscosity (sometimes called the 'compressional' or 'volume' viscosity). There have been a number of experimental measurements of the bulk viscosity of fluid argon[14,15], krypton[16] and xenon[15,17]. The experimental evidence from the work of Cowan *et al.*[14,17] and Baharudin *et al.*[16], is that, at constant pressure, the bulk viscosity increases with increasing temperature. This is observed for argon, krypton and xenon at pressures up to 60 atm. In stark contrast, the opposite behaviour is obtained for the MD simulated viscosities. (Both the experimental and simulation η_S decrease with increasing temperature.) At constant temperature the experimental bulk viscosity decreases with increasing pressure. This trend becomes stronger as temperature rises. Again, the opposite trend is observed for shear viscosity, both in experiment and simulation. The most comprehensive set of simulated bulk viscosities comes from Borgelt *et al.*[3] They observed a decrease in the bulk viscosity with increasing temperature at constant density. As the density (pressure) decreases, at constant temperature, the simulated bulk viscosity decreases, instead of increases, as happens in experiment. (Admittedly, the experimental Xe data does show some evidence of a reverse of this trend close to the triple point. But the simulations manifest a consistent trend at all temperatures as well as close to the triple point.) Therefore both the pressure and temperature dependence of the simulation bulk viscosity for LJ fluids is the opposite to that observed experimentally. The results of the present study confirm the previous simulation results. Before leaving

the topic of bulk viscosity we note that, unlike the shear viscosity, the bulk viscosity cannot be measured directly by experiment but must be extracted from ultrasonic attenuation in the fluids. The other fluid properties needed before this can be achieved are thermal conductivity, shear viscosity and the specific heat at constant pressure. Consequently it is a quantity for which greater uncertainty is to be expected. Nevertheless, the large body of different experiments and simulations does indicate a major fundamental discrepancy, which is extremely curious. Much of the interest in bulk viscosity has been centred on the triple point of the noble gas fluids. Both equilibrium and NEMD studies have been made at this state point[18–20]. The main point of interest here has been in η_S/η_B, which for experiment and simulation has a value of 0.33 ± 0.02. So in this number there is now a concensus of agreement. The behaviour of this ratio in these single component fluids in the predominantly higher temperature states more often studied is still in significant disagreement, however.

Mixtures have considerable practical and theoretical current interest. The purpose of the present work is to apply the same equilibrium MD techniques to binary fluid mixtures, with the objective of characterising the density and temperature dependence of the same transport coefficients. There has been some work performed on binary mixtures, but only at scattered state points and only calculating a limited number of transport coefficients (not always the same ones) at each state point considered. Mixtures have a distinct self-diffusion, D_v for each species or component, v, a shear viscosity, η_S, and thermal conductivity, κ. In these many-component mixtures there are additional transport coefficients to those of the single components, quantifying the mass flux and heat flux intermixing between the species. These clearly have no counterpart in the single component fluids and include the 'cross' transport coefficients, D^T, of thermal diffusion (the Soret effect) and the diffusion thermoeffect (the Dufour effect), which are numerically identical in the linear response regime according to the Onsager reciprocal relation. Molecular dynamics simulation has been used to calculate these[20–24]. The small magnitude of these thermo-diffusion coefficients gives rise to values with comparatively large percentage statistical uncertainties.

There is also the mutual diffusion coefficient, D_{12} which is mainly sensitive to the cross-species interactions as these are particularly influential in governing the interdiffusion of the total number of molecules of the two species. D_{12} has been evaluated by simulation for LJ[25–27], soft-sphere (SS)[28] and hard-sphere mixtures[29]. The accuracy of the D_{12} is considerably greater than that of the thermo-diffusion coefficients. These supplementary transport coefficients are calculated here using time cross-correlation functions in Green–Kubo expressions involving the excess thermodynamics of the mixture in their definition. In the case of mutual diffusion this appears as a multiplicative factor, Q, in the Green–Kubo integrand of the component momentum flux autocorrelation function. For the thermal conductivity and D^T, the heat flux *itself* has the component partial enthalpies in its definition, which is absent for a single component system[30]. In this study we determine the contribution of this enthalpic term to D^T and the thermal conductivity.

Simulation has also been used to determine the thermal conductivity and shear viscosity of model binary mixtures. Evans and Hanley,[31,32] and Murad[33,34] computed the shear viscosity of binary *SS* mixtures for several size and mass ratios.

In this study we concentrate on the transport coefficients of binary fluid mixtures, in the liquid Ar–Kr regime for which experimental[35] and some simulation data[20,21] already exists. We consider a more comprehensive set of state points than in previous work to calculate all of the mixture transport coefficients using the most recent statistical mechanical expressions for them. Our concern here is not in the mixing rules for the transport coefficients. more in the extent to which the MD model can simultaneously reproduce the transport coefficients of specific mixtures for which there is experimental data. Mikhailenko *et al.*[35] determined the bulk and shear viscosity of argon-krypton mixtures in the temperature range, 90–140 K over the full composition range. Consequently our simulations were carried out at the same state points. They found that the shear viscosity increased at constant temperature on going from pure argon to pure krypton. This is expected on corresponding states grounds, as the Kr is at a lower effective reduced temperature, k_BT/ε, where ε is the well-depth of the effective pair potential. The thermal conductivity manifests a more moderate increase as the mole fraction of Ar, $x_{Ar} \to 0$ at constant temperature. The bulk viscosity exhibits a completely different composition dependence. The η_B reaches a maximum at $x_{Ar} \sim 0.5$, which η_B being nearly equal for the pure argon and pure krypton at the same temperature (which would appear to defy corresponding states principles). We reveal that, as for single component fluids, there are significant differences between the simulated and experimental bulk viscosity.

2 THEORY AND SIMULATION METHOD

Fluid parameters

We consider a system of N_1 particles ('atoms') of mass m_1 and N_2 particles of mass m_2 contained in a volume V, mediated through a Lennard-Jones, LJ, (12-6) potential,

$$\phi_{\mu\nu}(r) = 4\varepsilon_{\mu\nu}((\sigma_{\mu\nu}/r)^{12} - (\sigma_{\mu\nu}/r)^6), \tag{1}$$

where μ and ν are the indices of the two species (i.e., ranging from 1 to 2). The cross-interactions governed by the generalised mixing rules,

$$\sigma_{12} = (\sigma_{11} + \sigma_{22})/2, \tag{2}$$

and,

$$\varepsilon_{12} = (\varepsilon_{11}\varepsilon_{22})^{1/2}, \tag{3}$$

These are the Lorentz–Berthelot mixing rules. The details of the simulation technique have been described elsewhere[2]. The MD simulations were performed using cubic unit cells of volume V containing mainly $N = 256$ Lennard-Jones (LJ) particles, although several simulations were conducted with $N = 108$ to assess the N-dependence of the properties. The interactions were truncated at half the box sidelength ($S/2$). We use both real and LJ reduced units (based on the parameters for species 1, which is *Ar*) in this report. For example, for temperature, $k_BT/\varepsilon_{11} \to T^*$, and number density, $\rho^* = N\sigma_{11}^3/V$. Reduced time is in units of $\sigma_{11}(m_1/\varepsilon_{11})^{1/2}$, viscosity in $(m_1\varepsilon_{11})^{1/2}/\sigma_{11}^2$, thermal conductivity in $k_B(m_1/\varepsilon_{11})^{-1/2}\sigma_{11}^{-2}$, self-diffusion coefficient in

Table 1 Molecular fluid parameters for the Lennard-Jones molecules used in the simulations, taken from Ref. [22].

Molecule	m_1/u	ε_{11}/k_B	σ_{11}/nm	m_1^*	ε_{11}^*	σ_{11}^*
			K			
Ar	39.95	119.8	0.3405	1	1	1
Kr	83.80	167.0	0.3633	2.0976	1.3940	1.06696

$\sigma_{11}(\varepsilon_{11}/m_1)^{1/2}$ and pressure tensor components in $\varepsilon_{11}\sigma_{11}^{-3}$. The time step, h, was typically ≈ 0.01 in reduced units. In Table 1 we give the LJ and real parameters for the model molecules considered in this work. Also in any study comparing simulation and experiment it is convenient to have interconversion factors to compare real and LJ reduced units. These we give in Table 2. Simulations performed on the CRAY-XMP at ULCC using *CFT77* were for typically $\sim 2 \times 10^5$ time steps in production for each state point.

Thermodynamic Properties

The mean configurational energy, U, of the N particles is accumulated as the time average,

$$U = \tfrac{1}{2} \sum_i^N \sum_j^N \phi_{ij} + N u_{lrc}, \tag{4}$$

Table 2 Conversion factors from reduced to real units, i.e., one combination of reduced units from the second column corresponds to the real units in the third and fourth columns. The reduced units, m, ε and σ are based on Ar, given in Table 1.

Quantity	*Reduced units*	*Coefficient*	*Real units*
Mass, m	m	6.6339	10^{-26} kg mol^{-1}
Time, t	$\sigma m^{1/2}\varepsilon^{1/2}$	2.1564	10^{-12} s
Number density, ρ	σ^{-3}	4.2063	10^{-2} mol cm^{-3}
Number density, ρ	σ^{-3}	9.4280	10^2 Amagat
Number density, ρ	σ^{-3}	1.6804	g cm^{-3} (Ar)
Number density, ρ	σ^{-3}	3.5249	g cm^{-3} (Kr)
Number density, ρ	σ^{-3}	2.6027	g cm^{-3} (0.5Ar + 0.5Kr)
Volume, V	σ^3	23.774	cm^3 mol^{-1}
Total Energy, E	ε	0.99607	kJ mol^{-1}
Pressure, P	$\varepsilon\sigma^{-3}$	41.898	MPa
Viscosity, η	$m^{1/2}\varepsilon^{1/2}\sigma^{-2}$	0.90349	10^{-4} Pas
Thermal cond., κ	$k_B m^{-1/2}\varepsilon^{1/2}\sigma^{-2}$	1.8803	10^{-2} Jm^{-1} K^{-1} s^{-1}
Diffusion coeff., D	$m^{-1/2}\varepsilon^{1/2}\sigma$	5.3765	10^{-8} m^2 s^{-1}
ρD	$m^{-1/2}\varepsilon^{1/2}\sigma^{-2}$	1.3619	10^{11} m^{-1} s^{-1}
ρD	$m^{-1/2}\varepsilon^{1/2}\sigma^{-2}$	5.0690	10^{-5} Amagat m^2 s^{-1}
ρD	$m^{-1/2}\varepsilon^{1/2}\sigma^{-2}$	1.8558 (T/K)(P/Atm)$^{-1}$	10^{-7} atmm^2 s^{-1}
D^T	$m^{1/2}\varepsilon^{1/2}\sigma^{-2}$	9.0349	10^{-5} m^{-1} s^{-1} kg

Note: k^T is dimensionless. An Amagat is the number density of an ideal gas at 1 atm and 0°C. (Ref: Collocot, T. C., and Dobson, A. B., *Dictionary of Science and Technology*, Chambers, 1974.) 1 Amagat $\equiv 1.06067 \times 10^{-3}\sigma^{-3}$.

where $N = N_1 + N_2$. For mole fractions, $x_1 = N_1/N$ and $x_2 = N_2/N$, and partial number densities, $\rho_\nu = N_\nu/V = x_\nu\rho$. The interactions need to be truncated at a separation, $r_c \leq S/2$. The long range corrections for $r_{ij} > r_c$ are,

$$u_{lrc} = u^r_{lrc} + u^a_{lrc}, \tag{5}$$

where

$$u^r_{lrc} = \frac{8\pi}{9r_c^9}\left[x_1\varepsilon_{11}\rho_1\sigma_{11}^{12} + 2x_1\varepsilon_{12}\rho_2\sigma_{12}^{12} + x_2\varepsilon_{22}\rho_2\sigma_{22}^{12}\right], \tag{6}$$

and

$$u^a_{lrc} = \frac{-8\pi}{3r_c^3}\left[x_1\varepsilon_{11}\rho_1\sigma_{11}^{6} + 2x_1\varepsilon_{12}\rho_2\sigma_{12}^{6} + x_2\varepsilon_{22}\rho_2\sigma_{22}^{6}\right]. \tag{7}$$

The lower case symbols denote intensive (i.e., per particle) quantities, whereas upper case symbols represent the extensive quantities for the entire system, e.g., $u = U/N + u_{lrc}$. Similarly, the mean enthalpy per particle is $h = H/N$, where

$$H = K_E + U + PV. \tag{8}$$

The kinetic energy per particle, $k_e = K_E/N$ is obtained from,

$$K_E = \tfrac{1}{2}\sum_\nu \sum_i^{N_\nu} p_{\nu i}^2/m_\nu, \tag{9}$$

where $p_{\nu i}$ is the momentum of particle i of species ν. The instantaneous temperature is,

$$T = 2K_E/(3N - 4)k_B. \tag{10}$$

The temperature and momenta are fixed, resulting in the removal of four degrees of freedom in Equation (10). The pressure is given by,

$$P = \frac{1}{3V}\left[\sum_\nu \sum_{i=1}^{N_\nu} p_{\nu i}^2/m_\nu - \sum_{i=1}^{N-1}\sum_{j>i}^{N} r\frac{d\phi(r_{ij})}{dr}\right] + P_{lrc}, \tag{11}$$

where the long-range correction to the pressure has a contribution from the repulsive (r) and attractive (a) components of the pair potential,

$$P_{lrc} = P^r_{lrc} + P^a_{lrc}, \tag{12}$$

where,

$$P^r_{lrc} = \frac{32\pi}{9r_c^9}\left[\varepsilon_{11}\rho_1^2\sigma_{11}^{12} + 2\varepsilon_{12}\rho_1\rho_2\sigma_{12}^{12} + \varepsilon_{22}\rho_2^2\sigma_{22}^{12}\right], \tag{13}$$

and

$$P^a_{lrc} = \frac{-16\pi}{3r_c^3}\left[\varepsilon_{11}\rho_1^2\sigma_{11}^{6} + 2\varepsilon_{12}\rho_1\rho_2\sigma_{12}^{6} + \varepsilon_{22}\rho_2^2\sigma_{22}^{6}\right]. \tag{14}$$

Partial molar quantities

The partial molar enthalpy is needed later to determine the exact expression for the heat flux. Below we outline the procedure for accomplishing this in an [NPT] ensemble MD simulation. For intensive property, $y = Y/N$, and mole fractions, x_i we have for an m-component mixture the partial thermodynamic quantity,

$$y_i = (\partial y/\partial x_i)_{x_j, T, P}. \tag{15}$$

From Euler's theorem we can relate the ensemble average thermodynamic quantity, y to these partial derivatives,

$$y = \sum_i^m x_i y_i. \tag{16}$$

For a binary system this reduces to,

$$y = x_1(\partial y/\partial x_1)_{x_2, T, P} + x_2(\partial y/\partial x_2)_{x_1, T, P}. \tag{17}$$

The total sum of the mole fractions, x is of course,

$$x = \sum_i^m x_i = 1. \tag{18}$$

If we define,

$$\begin{aligned} \Delta y &= (\partial y/\partial x_1)_{x, T, P} \\ &= (\partial y/\partial x_1)_{x_2, T, P} - (\partial y/\partial x_2)_{x_1, T, P} \\ &= y_1 - y_2. \end{aligned} \tag{19}$$

Therefore,

$$y_1 = y + (1 - x_1)\Delta y, \tag{20}$$

and,

$$y_2 = y - x_1 \Delta y. \tag{21}$$

These partial molar quantities have been evaluated for the specific enthalpy, h, and specific volume, $v = V/N$. We used the [NPT] ensemble to determine the partial thermodynamic quantities, using a recently proposed 'particle-swap' method for determining the Δy[14]. Each time step the energy change, ΔU, was evaluated, caused by replacing a particle by one of the other species without altering the configuration. For example, for the two species 1 and 2, the energy change on 'removing' a 1 atom and 'replacing' it by a 2 atom, ΔU^{2+1-},

$$\Delta U^{2+1-} = \sum_{\nu=1,2}^{2} \sum_{j_\nu \neq i_1} [\phi_{2\nu}(r_{i1j\nu}) - \phi_{1\nu}(r_{i1j\nu})]. \tag{22}$$

Also,

$$\begin{aligned} \Delta\mu &= \mu_1 - \mu_2 \\ &= \beta^{-1} \ln\langle \exp(-\beta \Delta U^{2+1-}) \rangle_{N_1, N_2} \end{aligned} \tag{23}$$

where $\beta = (k_B T)^{-1}$. In the simulation each particle in turn was chosen every time step as a candidate for this exchange. We also use Widom's particle insertion method to obtain μ_1 and μ_2 directly. If ΔU^{1^+} is the energy of a test particle of species 1 randomly inserted in the fluid,

$$\mu_1 = -\beta^{-1} \ln\langle \exp(-\beta \Delta U^{1^+}) \rangle_{N_2, T, P, N_1 - 1}, \tag{24}$$

The transposed expression (i.e., $1 \to 2$ and $2 \to 1$ in Equation (24) leads to an expression for μ_2). At every time step, we randomly positioned N_1 molecules of species 1 and N_1 molecules of species 2 in the fluid. Also,

$$\begin{aligned} \Delta h &= h_1 - h_2 \\ &= -\frac{\langle \Delta U^{2^+1^-} \exp(-\beta \Delta U^{2^+1^-}) \rangle_{N_1, N_2}}{\langle \exp(-\beta \Delta U^{2^+1^-}) \rangle_{N_1, N_2}} \\ &\quad - \frac{[\langle H \exp(-\beta \Delta U^{2^+1^-}) \rangle_{N_1, N_2} - \langle H \rangle_{N_1, N_2} \langle \exp(-\beta \Delta U^{2^+1^-}) \rangle_{N_1, N_2}]}{\langle \exp(-\beta \Delta U^{2^+1^-}) \rangle_{N_1, N_2}}, \end{aligned} \tag{25}$$

and for the volume,

$$\begin{aligned} \Delta v &= v_1 - v_2 \\ &= \frac{\langle V \exp(-\beta \Delta U^{2^+1^-}) \rangle_{N_1, N_2}}{\langle \exp(-\beta \Delta U^{2^+1^-}) \rangle_{N_1, N_2}} - \langle V \rangle_{N_1, N_2}. \end{aligned} \tag{26}$$

The [NPT] equations were introduced in the MD code by box sidelength and velocity rescaling procedures which were simple to implement and stable to arbitrary starting conditions (c.f. Ref. [36]). Constant temperature was achieved approximately using Woodcock's velocity rescaling procedure in a Verlet leapfrog algorithm[2]. For the desired temperature, T_0 and instantaneous temperature, T, (based on the half-time step momenta) we determine a momentum rescaling factor,

$$f = (T_0/T)^{1/2}, \tag{27}$$

$$\underline{p}(t + h/2) = \underline{p}(t - h/2) + \underline{F}(t)h, \tag{28}$$

where $\underline{F}$ is the systematic force. For each molecule, the new half-timestep velocity is rescaled, $\underline{p}(t + h/2) \to f\underline{p}(t + h/2)$. The Anderson constant pressure equations of motion were employed to establish an average pressure P_0 in the system. This can be rewritten as a series of rescaling operations applied to the molecular co-ordinates and velocities as follows. For a position, $\underline{r}$, and momentum, $\underline{p}$,

$$\dot{\underline{r}} = \underline{p} + \dot{\varepsilon}\underline{r}, \tag{29}$$

$$\dot{\underline{p}} = \underline{F} - \varepsilon \underline{\dot{p}}, \tag{30}$$

$$\dot{V} = (P - P_0)/M_A, \tag{31}$$

where the Anderson mass, $M_A = 0.005 m_1$, typically,

$$\ddot{\varepsilon} = \frac{\dot{V}}{3V}. \tag{32}$$

We use the velocity-Verlet algorithm to update the cell volume and implement Equations (29)–(32) in timesteps, h.

$$\dot{V}(t + h/2) = \dot{V}(t - h/2) + \ddot{V}(t)h, \tag{33}$$

$$V(t + h) = V(t) + \dot{V}(t + h/2)h, \tag{34}$$

$$\gamma = [V(t + h)/V(t)]^{1/3} - 1, \tag{35}$$

$$\underline{p}(t + h/2) \rightarrow [1 - \gamma]\underline{p}(t + h/2), \tag{36}$$

$$\underline{r}(t + h) = [1 + \gamma](\underline{r}(t) + \underline{p}(t + h/2)h). \tag{37}$$

The box sidelength $S = V^{1/3}$ is recalculated each time step to apply the periodic boundary conditions appropriate to the new MD cell dimensions. The long range corrections are also rescaled each time step,

$$u^r_{lrc} = u'^r_{lrc}(S'/S)^{12}, \tag{38}$$

$$u^a_{lrc} = u'^a_{lrc}(S'/S)^6, \tag{39}$$

$$P^r_{lrc} = P'^r_{lrc}(S'/S)^{15}, \tag{40}$$

$$P^a_{lrc} = P'^a_{lrc}(S'/S)^9, \tag{41}$$

where S' is the sidelength used to evaluate reference long range corrections, u'^r_{lrc}, u'^a_{lrc} P'^r_{lrc} and P'^a_{lrc}.

Each time step, the interaction truncation distance is scaled in proportion to S', in order to maintain the same molecules in each N-coordination shells after rescaling.

3 TRANSPORT COEFFICIENTS

In this section we discuss the formulae used to determine the transport coefficients of the system. The [NVT] ensemble was used in the molecular dynamics to determine the transport coefficients. The transport coefficients for a binary mixture of species, $\nu = 1, 2$, can be derived from the microscopically defined fluxes of matter, $\underline{J}_\nu$, and energy, $\underline{J}_Q$. Using and adapting the notation of MacGowan and Evans[21,22],

$$\underline{J}_\nu = N_\nu m_\nu(\underline{u}_\nu - \underline{u})/V, \tag{42}$$

where from the particle momenta, $\underline{p}_i$,

$$\underline{u}_\nu = \frac{1}{N_\nu m_\nu} \sum_i^{N_\nu} \underline{p}_i, \tag{43}$$

and,

$$\underline{u} = \sum_i^N \underline{p}_i/(N_1 m_1 + N_2 m_2). \tag{44}$$

As is conventional in a simulation, $\underline{u} = 0$ at the start of the simulation and it does

not deviate from this within machine error for the duration of the simulation. Hence, $J_1 = -J_2$ at all time, within machine error ($\sim 1{:}10^{-12}$).

The heat flux employed in the definition of the transport coefficients thermal conductivity and Soret (Dufour) coefficient, $\underline{J}_Q$, is defined as follows,

$$\underline{J}_Q = \underline{J}_{Q'} - \sum_\nu \underline{J}_\nu [h_\nu/m_\nu + \tfrac{1}{2}(J_\nu/m_\nu\rho_\nu)^2], \tag{45}$$

where h_ν is the specific partial enthalpy of species ν, evaluated using Equations (20) and (21). The term involving h_ν removes from the heat flux, $\underline{J}_{Q'}$, the enthalpy flux contribution associated with the interdiffusion of the one species through the other.

$$\underline{J}_{Q'} = \frac{1}{2V} \sum_\nu \sum_{i=1}^{N_\nu} [\{\underline{p}_i/m_\nu - \underline{u}\} m_\nu \{\underline{p}_i/m_\nu - \underline{u}\}^2 + \sum_j \{\underline{p}_i/m_\nu - \underline{u}\} \cdot (\phi_{ij}\underline{l} - \underline{q}_{ij}\underline{F}_{ij})]. \tag{46}$$

The momentum and position of particle i are $\underline{q}_i$ and $\underline{p}_i$, respectively, $\underline{q}_{ij}\underline{F}_{ij}$ is the dyad formed out of the two vectors.

The species or ν-dependent velocity (v) correlation function is,

$$C_{\nu\nu} = \frac{1}{3N_\nu} \sum_{i=1}^{N_\nu} [\underline{p}_i(0)/m_\nu - \underline{u}] \cdot [\underline{p}_i(t)/m_\nu - \underline{u}]. \tag{47}$$

The self-diffusion for each component is,

$$D_\nu = \int_0^\infty C_{\nu\nu}(t)dt. \tag{48}$$

Time correlation functions were integrated numerically by Simpson's rule to obtain the transport coefficients. As confirmation, the D_ν were evaluated also using the mean square displacements, $\zeta_\nu(t)$,

$$\zeta_\nu(t) = \sum_{i=1}^{N_\nu} [\underline{r}_i'(t) - \underline{r}_i(0)]^2/N_\nu. \tag{49}$$

In this function the particle positions, $\underline{r}_i'$ are not subjected to periodic boundary condition, PBC, shifts and can take on values outside the MD cell. (Particles always confined within the MD cell by applications of PBC are denoted by $\underline{r}_i(t)$). The self-diffusion for each component is then,

$$D_\nu = \frac{1}{6}\left[\frac{d\zeta_\nu(t)}{dt}\right]_{t\to\infty}. \tag{50}$$

The shear viscosity of the mixture is given by the following Green–Kubo relationship,

$$\eta = (V/k_B T) \int_0^\infty \langle P_{\alpha\beta}(0) P_{\alpha\beta}(t)\rangle dt, \tag{51}$$

where $P_{\alpha\beta}$ is the $\alpha\beta$ ($\alpha \neq \beta$) component of the pressure tensor, $\underline{P}$, which is,

$$P_{\alpha\beta} = \frac{1}{V}\left\{\sum_\nu \sum_{i=1}^{N_\nu} m_\nu [p_{\alpha i}/m_\nu - u_\alpha][p_{\beta i}/m_\nu - u_\beta] - \sum_{i=1}^{N-1} \sum_{j>i}^{N} (r_{\alpha ij} r_{\beta ij}/r_{ij}) \frac{d\phi(r_{ij})}{dr}\right\}, \tag{52}$$

where $r_{\alpha ij}$ is the α Cartesian component of $\underline{r}_{ij}$. Equation (52) is simply the m-species generalised formula used in single component fluids. The infinite frequency shear modulus of the mixture is given by the following fluctuation expression,

$$G_\infty = (V/k_B T)\langle P_{\alpha\beta}(0)\rangle^2. \tag{53}$$

The bulk viscosity of the mixture is given by the following Green–Kubo relationship,

$$\eta_B = (V/3k_B T)\int_0^\infty \langle (P(t) - \langle P\rangle)(P(0) - \langle P\rangle)\rangle dt. \tag{54}$$

The bulk modulus combination, $K_\infty - K_0$, of the mixture is given by the following fluctuation expression,

$$K_\infty - K_0 = (V/3k_B T)\langle (P - \langle P\rangle)^2. \tag{55}$$

The value of this quantity and also η_B will depend on the ensemble used to carry out the simulations. Here we employ [NVE] and [NVT] dynamics for all these quantities. At constant E, the adiabatic zero frequency bulk modulus K_0 will appear in Equation (55). At constant temperature, the isothermal bulk modulus will be the appropriate quantity. Quantities of current interest are the ratio of bulk to shear viscosity, η_B/η and the corresponding ratios if the moduli, $G_\infty/(K_\infty - K_0)$. These in turn lead to the phenomenological relaxation times, $\tau = \eta/G_\infty$ and $\tau_B = \eta_B/(K_\infty - K_0)$ which characterise the viscoelastic responses to small shear and volume strain distortions, respectively.

The thermal conductivity, κ is computed from,

$$\kappa = (V/k_B T^2)\int_0^\infty \langle J_{Q\alpha}(0)J_{Q\alpha}(t)\rangle dt, \tag{56}$$

where $J_{Q\alpha}$ is the α component of the heat flux, $\underline{J}_Q$. If we neglect the last term in Equation (45) as being insignificant (see the discussion) and let $a = -h_1/m_1$ and $b = -h_2/m_2$ then from (45) and (56) we can calculate three components of κ each determined by a different time correlation function,

$$\kappa = \kappa_{Q'Q'} + \kappa_{Q'J} + \kappa_{JJ}, \tag{57}$$

where,

$$\kappa_{Q'Q'} = (V/k_B T^2)\int_0^\infty \langle J_{Q'\alpha}(0)J_{Q'\alpha}(t)\rangle dt, \tag{58}$$

$$\kappa_{Q'J} = (2(a-b)V/k_B T^2)\int_0^\infty \langle J_{Q'\alpha}(0)J_{1\alpha}(t)\rangle dt, \tag{59}$$

$$\kappa_{JJ} = [(a-b)^2 V/k_B T^2]\int_0^\infty \langle J_{1\alpha}(0)J_{1\alpha}(t)\rangle dt, \tag{60}$$

making use of $J_1 = -J_2$. We see that as $a \to b$ the terms $\kappa_{Q'J}$, (63) and κ_{JJ}, (59) tend to zero. Therefore the formula for the single component fluid is recovered.

Equation (62) only remains, being the m-species generalised expression for the single component fluid.

The Soret, $\langle J_Q J_v \rangle$ and Dufour, $\langle J_v J_Q \rangle$ thermal diffusion coefficients are derived from,

$$D_s^T = \frac{V}{k_B T} \int_0^\infty \langle J_{Q\alpha}(0) J_{v\alpha}(t) \rangle dt, \tag{63}$$

$$D_D^T = \frac{V}{k_B T} \int_0^\infty \langle J_{v\alpha}(0) J_{Q\alpha}(t) \rangle dt. \tag{64}$$

By the principal of microscopic reversibility, $D_s^T = D_D^T$, which we simply denote by D^T here. Separating Equation (64) into the heat flux components as for κ we obtain,

$$D_s^T = D_{sQ'J}^T + D_{sJJ}^T, \tag{65}$$

where,

$$D_{sQ'J}^T = \frac{V}{k_B T} \int_0^\infty \langle J_{Q'\alpha}(0) J_{v\alpha}(t) \rangle dt, \tag{66}$$

$$D_{sJJ}^T = \frac{(a-b)V}{k_B T} \int_0^\infty \langle J_{v\alpha}(0) J_{v\alpha}(t) \rangle dt. \tag{67}$$

Equations of the same form apply for the decomposition of the Dufour coefficient, with Q' and J simply permuted.

The mutual diffusion coefficient, D_{12}, just as for D_v, can be calculated from a correlation function or an equivalent mean square displacement. We use both routes as a consistency check on the numerical computations.

$$Q^{-1} = 1 + \frac{\rho_1 \rho_2}{(\rho_1 + \rho_2)} (G_{11} + G_{22} - 2G_{12}), \tag{68}$$

where if $g_{v\mu}(r)$ is the species component pair radial distribution function,

$$G_{v\mu} = 4\pi \int_0^\infty r^2 dr (g_{v\mu}(r) - 1), \tag{69}$$

evaluated here using Simpson's rule. If,

$$\omega_v = N_v m_v / (N_1 m_1 + N_2 m_2), \tag{70}$$

then,

$$D_{12} = \frac{QV^2}{3N m_1 m_2 \omega_1 \omega_2} \int_0^\infty \langle J_1(0) J_1(t) \rangle dt. \tag{71}$$

An alternative form for D_{12} is from the average square of the distance that the centre of mass of species v particles moves in time t,

$$\zeta_v^{cm}(t) = \sum_{i=1}^{N_v} [\underline{r}_v^{cm}(t) - \underline{r}_v^{cm}(0)]^2, \tag{72}$$

where,

$$r_v^{cm} = \sum_{i=1}^{N_v} \underline{r}_i / N_v. \tag{73}$$

from which,

$$D_{12} = \frac{Q}{6Nm_1m_2\omega_1\omega_2} \left[\frac{d\zeta_v^{cm}(t)}{dt} \right]_{t\to\infty}. \tag{74}$$

From D_T and D_{12} we can define a dimensionless quantity, *thermal diffusion ratio*, k_T, as a measure of the relative importance of thermal and inter-diffusion,

$$k_T = c\left[\frac{D^T}{D_{12}}\right], \tag{75}$$

where,

$$c = \frac{\rho_1 m_1 + \rho_2 m_2}{\rho^2 m_1 m_2}. \tag{76}$$

The value of c is somewhat arbitrary. The above choice is the same as that of Hirschfelder *et al.*[20].

4 RESULTS AND DISCUSSION

Most of our simulations were conducted at zero applied pressure along two isotherms for variable Ar/Kr compositions. The two temperatures concentrated upon were $T = 120$ K and $T = 140$ K. (In LJ Ar reduced units, using the parameters from Table 1, these correspond to $T^* = 1.00167$ and $T^* = 1.16861$, respectively.)

Summaries of the state points considered and derived thermodynamic quantities from [NPT] simulations are given in Table 3. This table incorporates the average enthalpy per particle and the species-resolved chemical potentials. The corresponding partial quantities y_i for enthalpy and volume are given in Table 4. They are as statistically well-defined and N-independent as the thermodynamic averages given in Table 3. The table reveals that partial quantities are significantly less sensitive to composition than the average ensemble quantities (such as energy and enthalpy). The present LJ model accounts exceptionally well for the density of the mixtures at arbitrary composition, and also the effects of temperature. The essentially exact agreement between experiment[35] and simulation is demonstrated in Figure 1. It reveals that there is a near-linear relationship between the densities of the liquids between the extremes of pure Kr (on the left of the figure) and Ar (on the right of the figure).

We calculated the Ar–Kr binary mixture transport coefficients by simulation using the formulae described in the previous Section 3. As representative examples of the time correlation functions we show, in Figure 2, the x-cartesian component resolved momentum flux autocorrelation function of an equi-molar Ar–Kr mixture is shown.

Table 3 Thermodynamic quantities of the model liquid Ar–Kr mixtures at 1 Atm pressure in reduced units. The specific average enthalpies and chemical potentials of the two species from Equation (24) are given.

N	x_1	N_1	ρ	T	h	μ_1	μ_2
256	0.02344	6	0.68997	1.00167	−6.848	−3.15	−5.96
256	0.20312	52	0.69872	1.00167	−6.227	−3.36	−5.82
256	0.39844	102	0.7059	1.00167	−5.545	−3.40	−5.83
108	0.60185	65	0.71373	1.00167	−4.874	−3.40	−5.80
256	0.60156	154	0.71035	1.00167	−4.832	−3.45	−5.74
256	0.60156	154	0.71018	1.00167	−4.831	−3.46	−5.76
256	0.79687	204	0.70868	1.00167	−4.129	−3.50	−5.82
256	0.97656	250	0.70043	1.00167	−3.471	−3.49	−5.66
256	0.03906	10	0.64579	1.16861	−5.891	−3.01	−5.39
256	0.20312	52	0.64801	1.16861	−5.308	−3.09	−5.43
108	0.40741	44	0.64935	1.16861	−4.609	−3.09	−5.38
256	0.39844	102	0.64724	1.16861	−4.610	−3.15	−5.39
256	0.60156	154	0.63851	1.16861	−3.851	−3.18	−5.29
256	0.60156	154	0.63849	1.16861	−3.851	−3.18	−5.30
256	0.79687	204	0.61726	1.16861	−3.073	−3.17	−5.19
256	0.97656	250	0.56227	1.16861	−2.189	−3.10	−4.91

The negative region between $0.2 < t < 0.4$ may be a reflection of the 'back-scattering' events in the velocity autocorrelation function component of the flux autocorrelation function. The time integral of the flux is presented in Figure 3. In Figure 4 we show the associated stress autocorrelation functions for the same state point (i.e., P_{xy}, P_{xz} and P_{yz}). As is typical for stress tensor component autocorrelation functions they

Table 4 Partial Mixing Properties of model liquid Ar–Kr mixtures at 1 Atm pressure by simulation in reduced units. The partial enthalpies are obtained using [NPT] dynamics and equations (20) and (21).

N	x_1	N_1	ρ	T	h_1	h_2	v_1	v_2
256	0.02344	6	0.68997	1.00167	−3.53	−6.93	1.35	1.45
256	0.20312	52	0.69872	1.00167	−3.54	−6.91	1.36	1.45
256	0.39844	102	0.7059	1.00167	−3.48	−6.91	1.38	1.44
108	0.60185	65	0.71373	1.00167	−3.46	−7.01	1.40	1.41
256	0.60156	154	0.71035	1.00167	−3.42	−6.97	1.40	1.42
256	0.60156	154	0.71018	1.00167	−3.42	−6.96	1.40	1.42
256	0.79687	204	0.70868	1.00167	−3.41	−6.97	1.42	1.38
256	0.97656	250	0.70043	1.00167	−3.38	−7.08	1.43	1.29
256	0.03906	10	0.64579	1.16861	−2.48	−6.03	1.51	1.55
256	0.20312	52	0.64801	1.16861	−2.51	−6.02	1.53	1.55
108	0.40741	44	0.64935	1.16861	−2.48	−6.07	1.57	1.52
256	0.39844	102	0.64724	1.16861	−2.45	−6.04	1.58	1.53
256	0.60156	154	0.63851	1.16861	−2.35	−6.11	1.63	1.47
256	0.60156	154	0.63849	1.16861	−2.38	−6.12	1.63	1.47
256	0.79687	204	0.61726	1.16861	−2.22	−6.43	1.71	1.27
256	0.97656	250	0.56227	1.16861	−2.05	−8.04	1.83	0.06

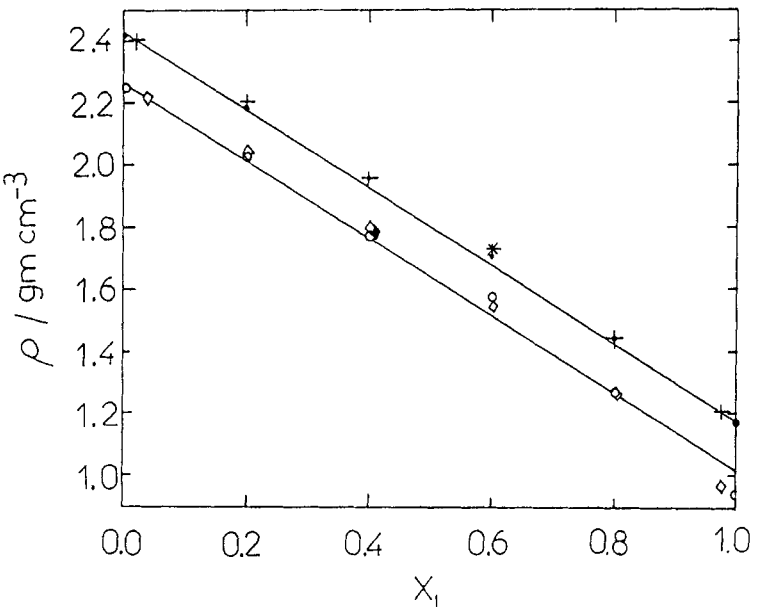

Figure 1 The dependence of the density of the liquid on the mole fraction, x_1 of Ar. Key: Experiment, ● $T = 120$ K, ○ $T = 140$ K; simulation results, +, $N = 256$ $T = 120K$, ×, $N = 108$, $T = 120$ K, ◇, $N = 256$ $T = 140$ K, ◆, $N = 108$, $T = 140$ K.

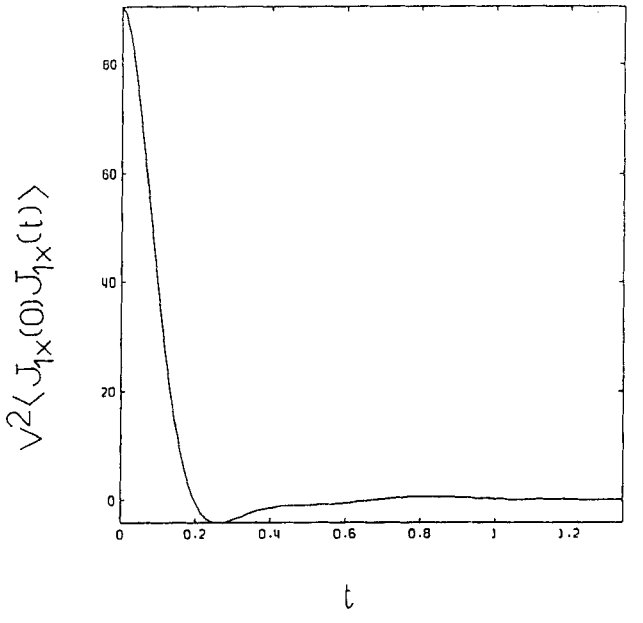

Figure 2 The flux autocorrelation function, $V^2\langle J_{1\alpha}(0)J_{1\alpha}(t)\rangle$ for a model Ar–Kr mixture with $x_1 = 0.60156$, $\rho^* = 0.71018$ and $T^* = 1.00167$.

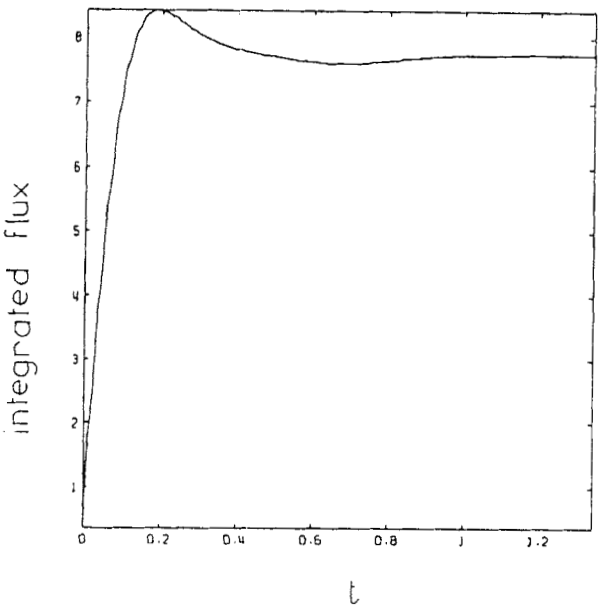

Figure 3 As for Figure 2, except the integrated flux is given.

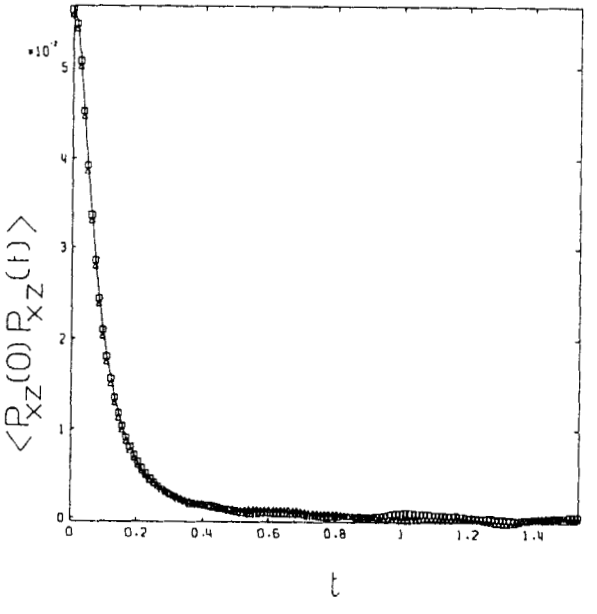

Figure 4 As for Figure 2, except that the shear stress autocorrelation function, $\langle P_{\alpha\beta}(0)P_{\alpha\beta}(t)\rangle$, is given. Key: $\alpha\beta = xy$, □; $\alpha\beta = xz$, ——; $\alpha\beta = yz$, △.

show a more monotonic decay with no noticeable negative lobe at $t \sim 0.2$. The integrated time dependent shear viscosity from Equation (51) is given Figure 5.

We carried out simulations on model pure argon to determine the ensemble dependence of the transport coefficients. We considered [NVE] and [NVT] ensembles. The table 5 reveals that the only transport coefficient manifesting a significant ensemble dependence is the bulk viscosity. The [NVE] values are smaller, largely due to a smaller $K_\infty - K_0$ in the [NVE] case rather than at [NVT]. At constant E the relevant zero frequency modulus, K_0 is the adiabatic quantity, whereas at constant temperature we have the isothermal K_0. Nevertheless, with both isothermal and isoenergetic simulations the bulk viscosity decreases with increasing temperature, the opposite trend to experiment (as discussed in the Introduction). It is reasonable that the temporal nature of pressure fluctuations will be sensitive to the ensemble of the simulation. The table reveals that (apart from the diffusion coefficients) all the moduli and transport coefficients diminish with increasing temperature at fixed pressure.

In Figure 6 we show the bulk viscosity autocorrelation function from an [NVE] simulation, and its time-integral in Figure 7. In order to obtain the correlation function of Equation (54) from $\langle P(0)P(t)\rangle$ we need to subtract off $t \to \infty$ of $\langle P(0)P(t)\rangle$. For correlation functions persisting for 200 time steps we take the average of $\langle P(0)P(t)\rangle$ over the last n time steps of the duration of the correlation function. In Figures 6 and 7 we show the effects of using $n = 25$, 50 and 75. The figures reveal that there is little statistical difference between them. In Figure 8 we show the J_Q

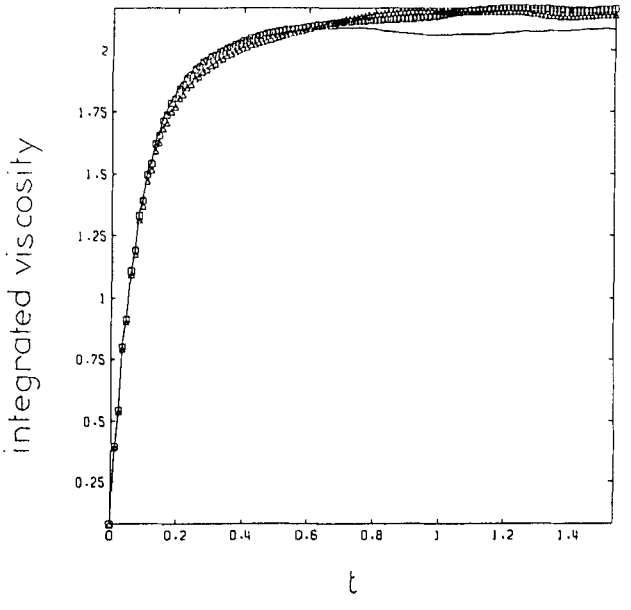

Figure 5 As for Figure 4, except the corresponding integrated viscosities are shown.

Table 5 Transport coefficients of model LJ Ar in reduced units. The statistical uncertainty is ± 5%. All calculations were carried out at constant temperature, in the [NVT] ensemble, except the rows denoted by † which denote [NVE] ensemble simulations. $N = 256$.

ρ	T	G_x	η_s	$K_x - K_0$	η_B	κ	ρD
0.8442	0.722	23.09	3.27	24.63	2.98	6.73	0.0254
0.8442	0.774	26.14	3.28	13.71	1.03	7.90	0.0282†
0.715	0.915	17.81	1.61	21.21	1.70	5.30	0.0556
0.715	0.896	17.13	1.67	12.40	0.74	4.95	0.0544†
0.570	1.20	9.98	0.73	10.53	0.83	3.04	0.1184†

autocorrelation functions for a near equi-molar mixture. The corresponding integrated thermal conductivity is given in Figure 9.

In Table 6 we present the transport coefficients derived from these simulations. We have conducted an isolated simulation at a near-triple point state to compare with a previous simulation[20]. Agreement is good for the shear viscosity and thermal conductivity but the present simulations produce a value for the bulk viscosity approximately double the value of the previous work. This is expected, given the evidence of Table 5, as [NVT] dynamics was used for the present study at this isolated

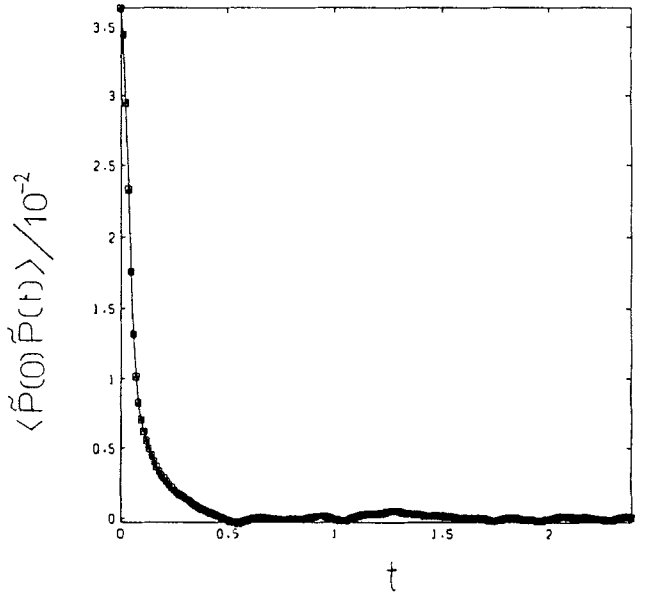

Figure 6 The pressure deviation autocorrelation function, $C_B(t) = \langle (P(t) - \langle P \rangle)(P(0) - \langle P \rangle) \rangle$, where $\tilde{P} = P - \langle P \rangle$. The $\langle P \rangle^2$ are taken from the long time value of $\langle P(t)P(0) \rangle$ averaged over (a) the last 75 time steps, ———, (b) □ the last 50 time steps and (c) the last 25 time steps. △. (The correlation function extends for 200 time steps.) The state point is $\rho = 0.70868$, $T = 1.0027$ using [NVE] dynamics from the correlation functions from Figure 6 and Equation (54).

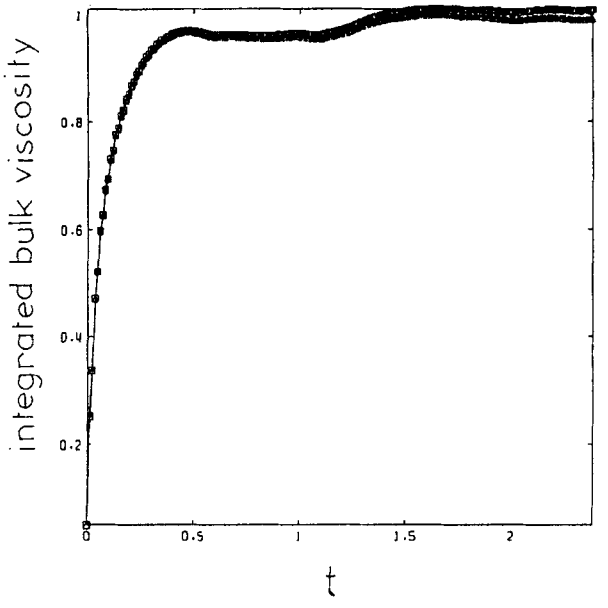

Figure 7 As for Figure 6, except that the time integrated bulk viscosity is shown.

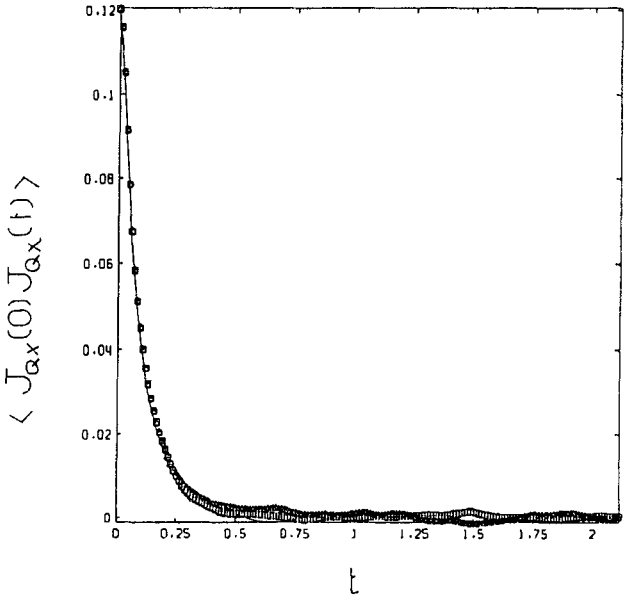

Figure 8 The heat flux autocorrelation function, $\langle J_{Q\alpha}(0)J_{Q\alpha}(t)\rangle$ for a model Ar–Kr mixture with $x_1 = 0.60156$, $\rho^* = 0.71018$ and $T^* = 1.00167$. Key: $\alpha = x$, □; $\alpha = y$, ——; $\alpha = z$, △.

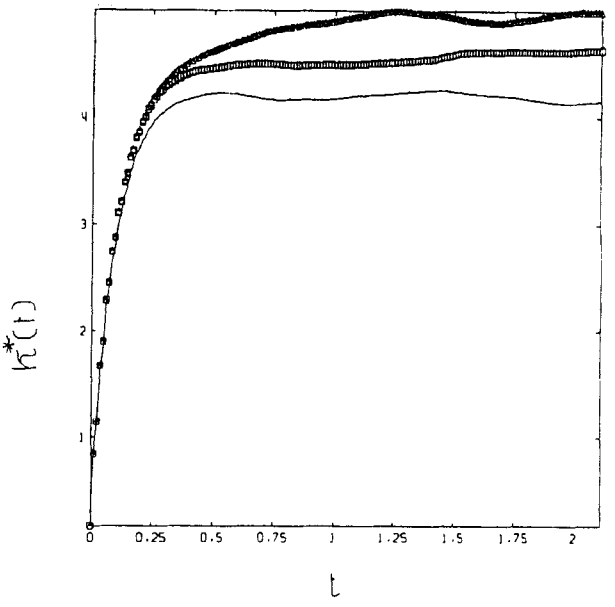

Figure 9 As for Figure 8, except that the integrated thermal conductivities are given.

Table 6 Transport coefficients of model binary mixtures of model LJ Ar–Kr reduced units. The statistical uncertainty is ±5%. All calculations were carried out at constant temperature, i.e., in the [NVT] ensemble, except the results in the rows denoted by † which were derived in the [NVE] ensemble. Key: simulation * Ref. [8].

N	x_1	ρ	T	G_x	η_s	$K_x - K_0$	η_B	κ
256	0.5	0.703	0.968	20.41	2.35	23.55	2.52	4.21
256*	0.5	0.703	0.968	—	2.27	—	1.12	4.22
256	0.02344	0.68997	1.0017	26.11	4.26	27.35	3.62	4.82
256	0.02344	0.68997	1.0204	26.70	4.55	14.53	1.70	4.82†
256	0.20312	0.69872	1.0017	24.64	3.61	25.74	3.03	4.70
256	0.39844	0.70597	1.0017	22.32	2.63	24.72	2.34	4.13
256	0.39844	0.70597	0.9845	21.88	2.84	14.11	1.64	4.63†
108	0.60185	0.71373	1.0017	20.27	2.09	23.59	2.21	4.48
256	0.60156	0.71018	1.0017	20.24	2.20	23.29	2.16	4.59
256	0.79687	0.70868	1.0017	17.65	1.58	21.22	1.62	4.55
256	0.79687	0.70868	1.0027	17.86	1.66	13.11	0.99	4.35†
256	0.97656	0.70043	1.0017	15.48	1.27	19.20	1.23	4.54
256	0.97656	0.70043	0.9915	15.09	1.25	12.63	1.06	4.59†
256	0.03906	0.64579	1.16861	22.10	2.84	25.42	2.83	3.94
256	0.03906	0.64579	1.1555	21.81	2.86	14.51	1.33	3.49†
256	0.20312	0.64801	1.16861	20.50	2.21	23.92	2.05	3.80
256	0.39844	0.64724	1.16861	18.04	1.82	22.55	1.92	3.46
256	0.39844	0.64724	1.1427	17.66	1.82	13.45	1.00	3.37†
256	0.60156	0.63850	1.16861	15.57	1.38	19.70	1.53	3.67
256	0.79687	0.61726	1.16861	12.78	0.98	16.86	0.88	3.30
256	0.79687	0.61726	1.1867	13.26	1.07	12.38	1.12	3.49†
108	0.97222	0.56227	1.16861	9.30	0.69	12.65	0.78	2.68
256	0.97656	0.56227	1.16861	9.37	0.68	12.83	0.60	2.59
256	0.97656	0.56227	1.1747	9.43	0.70	10.48	1.09	2.82†

state point and [NVE] dynamics for the previous work. Support for the present algorithm is found in a comparison between the bulk viscosities of the higher temperature state points produced by these simulations and the experimental values[19] discussed below. In Figure 10 we compare the experimental and simulation shear viscosities in real units at $T = 120$ K and $T = 140$ K and as a function of composition. As expected, the viscosities decrease in magnitude as the argon content increases, because the pure krypton liquid is at an effectively lower T^* than the argon at the same absolute temperature (K). The simulation and experimental values for η_s are statistically indistinguishable, following an approximate linear relationship with composition between the two pure liquids.

Also for the bulk viscosity, the value decreases as pure argon is approached, shown in Figure 11. The experimental bulk viscosities are of similar magnitude (as $x_{Ar} \to 0$) but show a more flat composition dependence. The shear moduli (Figure 12) and relaxation times (Figure 13) obtained by the simulations are in very good agreement with the experimental values. In the case of the moduli there is again a near-linear composition dependence, whereas there is a more gradual variation in the shear relaxation time in the pure argon limit. In Figure 14 it is evident that experimental values for the times τ_B are about to double the simulation values, increasing as pure argon is approached. These experimental results seems counter intuitive as relaxation times would be expected to increase for the more attractive component.

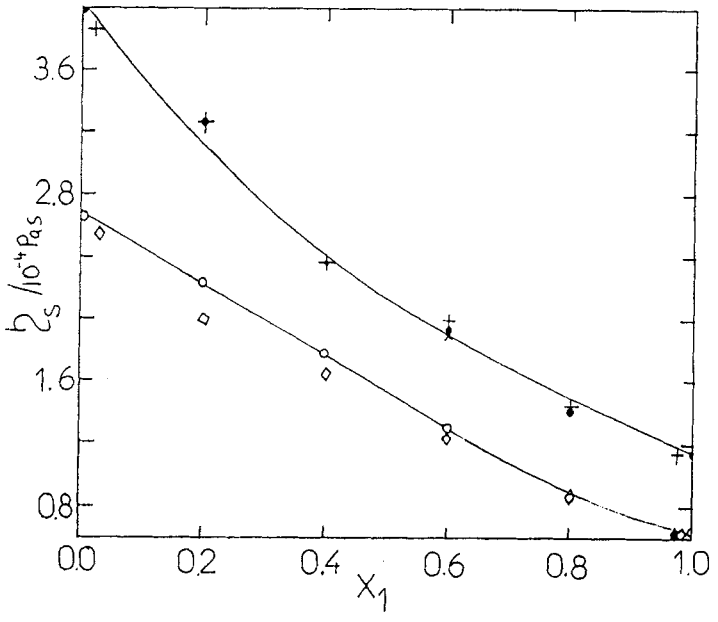

Figure 10 The dependence of the shear viscosity of the liquid on the mole fraction, x_1 of Ar. Key: Experiment, ● $T = 120$ K, ○ $T = 140$ K; simulation results, +, $N = 256$ $T = 120$ K, ×, $N = 108$, $T = 120$ K, ◇, $N = 256$ $T = 140$ K, ◆, $N = 108$, $T = 140$ K.

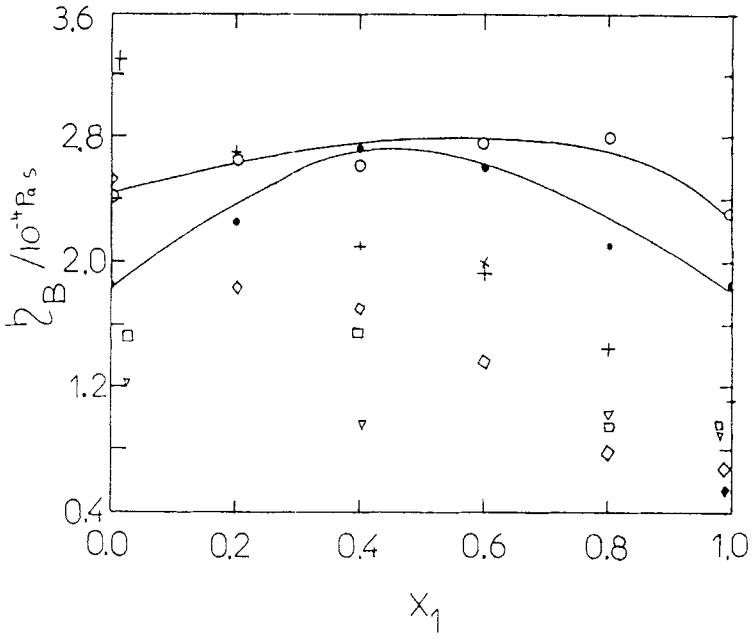

Figure 11 The dependence of the bulk viscosity of the liquid on the mole fraction, x_1 of Ar. Key: Experiment, ● $T = 120$ K, ○ $T = 140$ K; simulation results, +, $N = 256$ $T = 120$ K, ×, $N = 108$, $T = 120$ K, ◇, $N = 256$ $T = 140$ K, ◆, $N = 108$, $T = 140$ K.

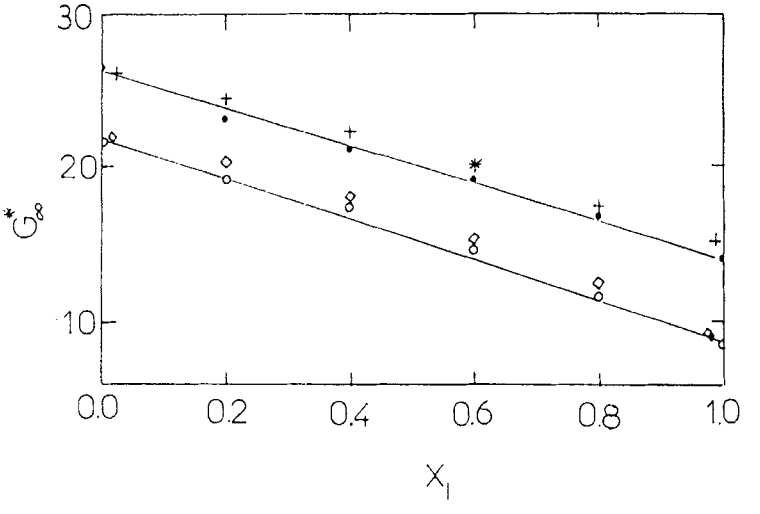

Figure 12 The dependence of the shear modulus of the liquid on the mole fraction, x_1 of Ar. Key: Experiment, ● $T = 120$ K, ○ $T = 140$ K; simulation results, +, $N = 256$ $T = 120$ K, ×, $N = 108$, $T = 120$ K, ◇, $N = 256$ $T = 140$ K, ◆, $N = 108$, $T = 140$ K.

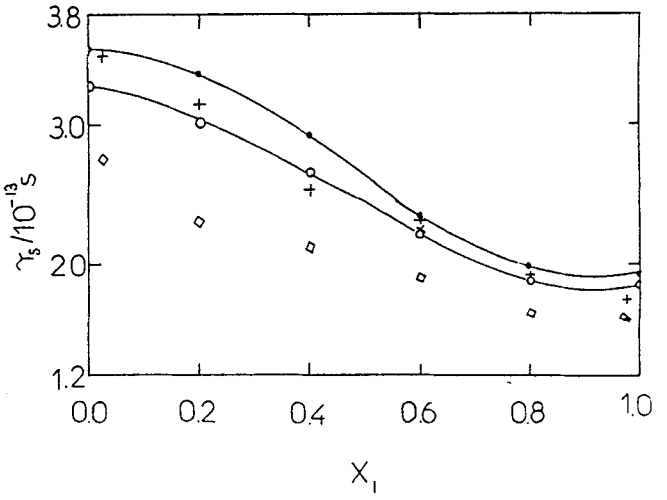

Figure 13 The dependence of the shear relaxation time of the liquid on the mole fraction, x_1 of Ar. Key: Experiment, ● $T = 120$ K, ○ $T = 140$ K; simulation results in the [NVT] ensemble, +, $N = 256$ $T = 120$ K, ×, $N = 108$, $T = 120$ K, ◇, $N = 256$ $T = 140$ K, ◆, $N = 108$, $T = 140$ K. [NVE] at $N = 256$ at $T = 120$ K is □ and $T = 140$ K $N = 256$ ▽.

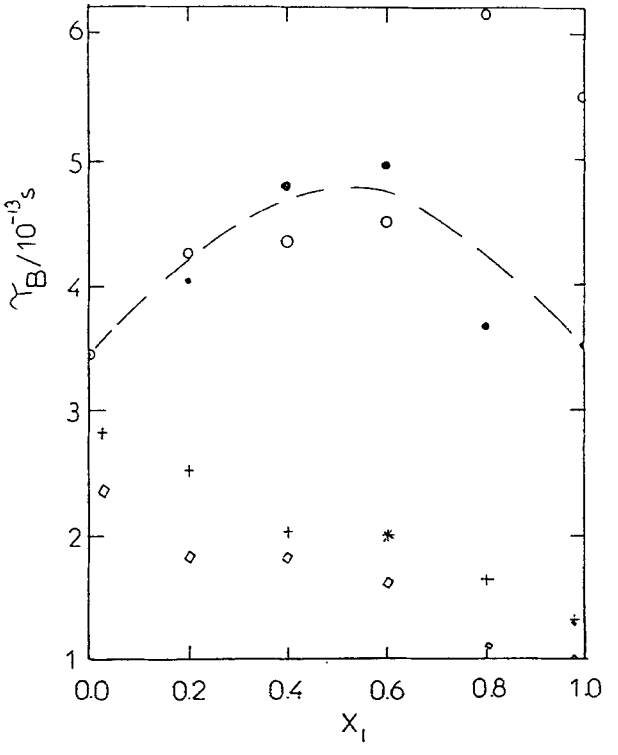

Figure 14 The dependence of the bulk relaxation time of the liquid on the mole fraction, x_1 of Ar. Key: Experiment, ● $T = 120$ K, ○ $T = 140$ K; simulation results, +, $N = 256$ $T = 120$ K, ×, $N = 108$, $T = 120$ K, ◇, $N = 256$ $T = 140$ K, ◆, $N = 108$, $T = 140$ K all at [NVT].

Table 5 shows that the thermal conductivity of the Ar/Kr states at $T = 120$ K are insensitive to the composition, whereas at $T = 140$ K we observe a more dramatic decrease as Kr → Ar in the mixture. For these dense fluids we note that the m-component generalisation of the single component heat flux formula of Equation (58) gives statistically the same results as the exact formula (56). This is because the terms $\kappa_{Q'J}$ and κ_{JJ} are numerically small. The agreement between simulation and experimental values for the thermal conductivity is exceptional, as revealed in Figure 15.

Table 6 reviews diffusion coefficients and thermal transport coefficients of the mixtures. At the near-triple point state ($\rho = 0.703$ and $T = 0.968$, in reduced units) the self- and mutual diffusion coefficients are statistically indistinguishable between this and a previous simulation[8]. As has been found elsewhere,[8,9] $\rho D_{12}/(\rho_1 D_1 + \rho_2 D_2) \simeq 1$. Otherwise, we simply present the numbers for future reference, in the absence of any experimental data to compare with.

We discovered that there are some differences between the Soret and Dufour coefficients evaluated by MD using the present correlation function approach. These cross thermodiffusion coefficients are extremely difficult to obtain by simulation, as the cross-correlation functions are more sensitive to the algorithm used to integrate the equations of motion than those of the autocorrelation functions. Consequently their integral is more susceptible to such errors. As in this previous study[8], an average of the two was taken as the best estimate of the thermal diffusion coefficients i.e., $D^T = (D_s^T + D_D^T)/2$. We again give the values for D^T and k_T for future reference when experiments are performed on these systems. We give the values of D^T and k_T in

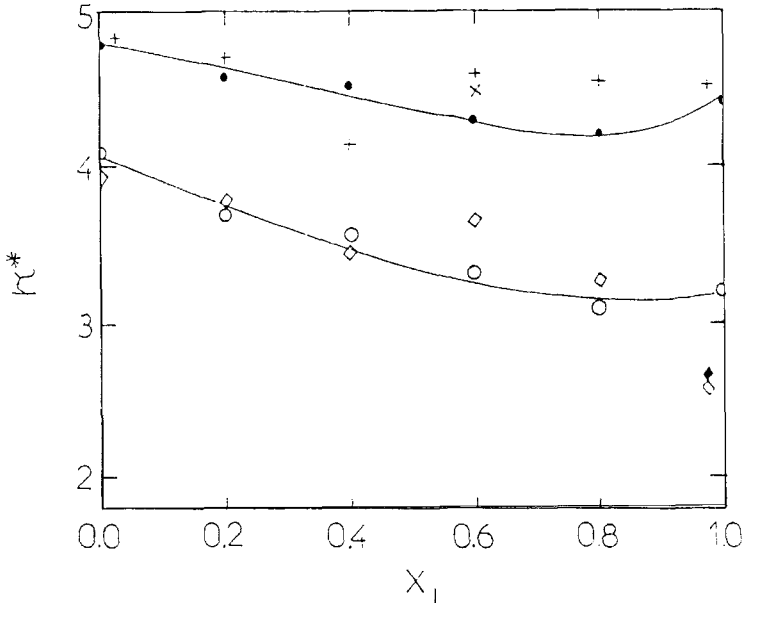

Figure 15 As for Figure 11, except that the thermal conductivity is considered, again at [NVT].

Table 7 Transport coefficients of model binary mixtures of model LJ Ar–Kr reduced units. The statistical uncertainty is ±5% for the $\rho_i D_i$ and ρD_{12} but ~30% for D^T and k_T. Key: simulation * Ref. [8]. All simulations are [NVT] except those in the rows denoted by † for which [NVE] dynamics was used.

N	x_1	ρ	T	$\rho_1 D_1$	$\rho_2 D_2$	ρD_{12}	$D^T/0.01$	k_T
256	0.5	0.703	0.968	0.0201	0.0164	0.0388	−1.61	−0.31
256*	0.5	0.703	0.968	0.0212	0.0170	0.0366	−0.885	—
256	0.02344	0.68997	1.0017	0.000569	0.0192	0.0250	0.15	0.059
256	0.02344	0.68997	1.0204	0.000564	0.0197	0.0249	−0.086	−0.0345†
256	0.20312	0.69872	1.0017	0.00805	0.0187	0.0306	−1.25	−0.36
256	0.39844	0.70597	1.0017	0.0144	0.0180	0.0355	−0.941	−0.21
256	0.39844	0.70597	0.98451	0.0142	0.0176	0.0330	−2.70	−0.64†
108	0.60185	0.71373	1.0017	0.0257	0.0138	0.0391	−2.67	−0.467
256	0.60156	0.71018	1.0017	0.0275	0.0150	0.0422	−2.92	−0.475
256	0.79687	0.70868	1.0017	0.0458	0.00953	0.0504	−2.23	−0.257
256	0.79687	0.70868	1.0017	0.0458	0.00955	0.0529	−2.22	−0.24†
256	0.97656	0.70043	1.0017	0.0690	0.00133	0.0587	−0.62	−0.051
256	0.97656	0.70043	1.0017	0.0682	0.00134	0.0571	−0.40	−0.30†
256	0.03906	0.64579	1.16861	0.00156	0.0311	0.0419	−0.33	−0.076
256	0.03906	0.64579	1.1555	0.00153	0.0309	0.0377	0.030	0.0078†
256	0.20312	0.64801	1.16861	0.00955	0.0307	0.0469	−1.75	−0.33
256	0.39844	0.64724	1.16861	0.0229	0.0283	0.0544	−1.57	−0.23
256	0.39844	0.64724	1.1427	0.0223	0.0273	0.0540	−3.05	−0.44†
256	0.60156	0.63850	1.16861	0.0426	0.0229	0.0673	−5.45	−0.547
256	0.79687	0.61726	1.16861	0.0710	0.0146	0.0785	−6.01	−0.44
256	0.79687	0.61726	1.1867	0.0716	0.0147	0.0820	−5.7	−0.40†
108	0.97222	0.56227	1.16861	0.106	0.00233	0.0861	−2.70	−0.15
256	0.97656	0.56227	1.16861	0.110	0.00213	0.0960	−1.62	−0.08
256	0.97656	0.56227	1.1747	0.111	0.00208	0.0930	−2.3	−0.12†

Table 7 for reference, acknowledging that there are large percentage uncertainties in the simulation values.

5 CONCLUSIONS

In this report we have applied a time correlation function approach to obtain the transport coefficients of some model binary mixtures, for the first time using the correct definition of the heat flux, which is needed for over half of the transport coefficients. This expression uses the partial enthalpy of the two species, which were obtained from parallel constant pressure simulations at the same state points as the simulations used to compute the transport coefficients. It transpires that the contribution of the enthalpy term to the thermal conductivity is small in practice because the magnitude of the extra terms it introduces in the definition of the thermal conductivity are numerically small at these densities.

Most of the simulations were performed along two isotherms to compare with a previous experimental study of the dense fluid Ar–Kr mixtures. This is a region of the phase diagram well-suited to MD as the correlation functions decay within the

~ 5 psec followed in these simulations (this is a typical upper time limit on the duration of the time correlation functions that can be followed with statistical certainty at these densities). Therefore the derived transport coefficients (obtained from Green–Kubo integration) are obtained free of 'long-time tails' which can make such studies impractical at low density and in the region of glassy behaviour. (The temperatures are sufficiently high at these densities to exclude any such viscous behaviour.)

A detailed comparison with the experimental study of Mikhailenko *et al.*[35] reveals exceptional agreement between the simulation and experimental values for the average densities of the mixtures at the mole fractions considered. The shear viscosities and infinite frequency shear moduli are in very good agreement also. The simulation bulk viscosities show a variation with composition more in line with the shear viscosities (Diminishing with temperature increase and Ar content). However, the experimental bulk viscosities have a rather flat variation with composition. The experimental and simulation thermal conductivities agree well over all compositions and temperatures studied.

We also calculated the species component self-diffusion and mutual diffusion coefficients, and the thermotransport coefficients for these compositions, at this stage, largely for future reference as there is no experimental data available to compare with at present. The thermodiffusion coefficients have large statistical uncertainty by the Green–Kubo method of this study, but both are usually negative.

Acknowledgements

D.M.H. gratefully thanks *The Royal Society* for the award of a *Royal Society 1983 University Research Fellowship*. We thank D. MacGowan for helpful discussions. We express gratitude to the S.E.R.C. for the award of computer time on the CRAY-XMP at the University of London Computer Centre, and the RHBNC Computer Centre also for use of their computing facilities.

References

1. J.-P. Ryckaert, A. Bellemans, C. Ciccotti and G. V. Paolini, *Phys. Rev. A*, **39**, 259 (1989).
2. D. M. Heyes, *Phys. Rev. B*, **37** 5677 (1988).
3. P. Borgelt, C. Hoheisel and G. Stell, *Phys. Rev. A*, **42**, 789 (1990).
4. B. J. Alder, D. M. Gass, and T. E. Wainwright, *J. Chem. Phys.*, **53**, 3813 (1970).
5. D. Levesque, L. Verlet, and J. Kurkijarvi. *Phys. Rev. A*, **7**, 1690 (1973).
6. C. G. Joslin, C. G. Gray, J. P. J. Michels and J. Karkheck, *Mol. Phys.*, **69**, 535 (1990).
7. G. Ciccotti, W. G. Hoover, C. Massobrio, and G. V. Paolini, *Phys. Rev. A*, **36**, 3471 (1987).
8. J. P. Ryckaert, A. Bellemans, G. Ciccotti, and G. V. Paolini, *Phys. Rev. Lett.*, **60**, 128 (1988).
9. J.-P. Ryckaert, A. Bellemans, G. Ciccotti and G. Paolini, *Phys. Rev. A*, **39**, 259 (1989).
10. D. J. Evans and G. P. Morriss, *Statistical Mechanics of Nonequilibrium liquids*, Academic Press, 1990.
11. D. M. Heyes, *JCS Faraday Trans II*, **82**, 1365 (1986).
12. J. J. van Loef and E. G. D. Cohen, *Physica A*, **156**, 522 (1989).
13. P. W. E. Peereboom, H. Luigjes and K. O. Prins, *Physica A*, **156**, 260 (1989).
14. J. A. Cowan and P. W. Ward, *Can. J. Phys.*, **51**, 2219 (1973).
15. P. Malbrunot, A. Boyer, E. Charles and H. Abachi, *Phys. Rev. A*, **27**, 1523 (1983).
16. B. Y. Baharudin, D. A. Jackson, P. E. Schoen and J. Rouch, *Phys. Lett. A*, **51** 409 (1975).
17. J. A. Cowan and J. W. Leech, *Can. J. Phys.*, **59**, 1280 (1981).
18. W. G. Hoover, A. J. C. Ladd, R. B. Hickman and B. L. Holian, *Phys. Rev. A*, **21**, 1756 (1980).
19. W. G. Hoover, D. J. Evans, R. B. Hickman, A. J. C. Ladd, W. T. Ashurst and B. Moran, *Phys. Rev. A*, **22**, 1690 (1980).

20. C. Hoheisel and R. Vogelsang, *Comp. Phys. Rep.*, **8**, 1 (1988).
21. D. MacGowan and D. J. Evans, *Phys. Rev. A*, 1986 **34**, 2133 (1986).
22. D. J. Evans and D. MacGowan, *Phys. Rev. A*, **36**, 948 (1987).
23. D. MacGowan, *Phys. Rev. A*, **36**, 1367 (1987).
24. K. Nakanishi, H. Narusawa and K. Toukubo, *J. Chem. Phys.* **72**, 3089 (1980).
25. R. Vogelsang, and C. Hoheisel, *J. Chem. Phys.*, **89**, 1588 (1988).
26. M. Schoen and C. Hoheisel, *Mol. Phys.*, **52**, 33; **52**, 1029 (1984).
27. J. M. Stoker, and R. L. Rowley, *J. Chem. Phys.*, **91**, 3670 (1989).
28. B. Bernu, J.-P. Hansen, Y. Hiwatari, and G. Pastore, *Phys. Rev. A*, **36**, 4891 (1987).
29. J. M. Kincaid, and J. J. Erpenbeck, *J. Chem. Phys.*, **84**, 3418 (1986).
30. P. Sindzingre, C. Masobrio, G. Ciccotti, and D. Frenkel, *Chem. Phys.* **136** 213 (1989).
31. D. J. Evans, and H. J. M. Hanley, *Phys. Rev. A.*, **20**, 1648 (1979).
32. H. J. M. Hanley and D. J. Evans, *Mol. Phys.*, **39**, 1039 (1980).
33. S. Murad, D. P. S. Sethi, and P. V. Ravi, *Fluid Phase Equilibria* **53**, 159 (1989).
34. S. Murad, *AlChE Journal*, **35**, 311 (1989).
35. S. A. Mikhailenko, V. G. Dudar, V. N. Derkach, and V. N. Zozulya, *Sov. J. Low Temp. Phys.*, **3**, 331 (1977).
36. B. L. Holian, A. J. De Groot, W. G. Hoover and C. G. Hoover, *Phys. Rev. A*, **41**, 4552 (1990).